6th European Conference on Computational Mechanics (ECCM 6)
7th European Conference on Computational Fluid Dynamics (ECFD 7)
1115 June 2018, Glasgow, UK

AN ADAPTIVE ALGORITHM TO ACCELERATE THE CRITICAL PLANE IDENTIFICATION FOR MULTIAXIAL FATIGUE CRITERIA

MICHAEL WENTINGMANN[1], PABLO NOEVER-CASTELOS[1] AND CLAUDIO BALZANI[1]

[1] Leibniz Universität Hannover
Institute for Wind Energy Systems
Appelstraße 9 A, 30167 Hannover, Germany
www.iwes.uni-hannover.de
research@iwes.uni-hannover.de

Key words: adaptive algorithm, critical plane, multiaxial fatigue, non-proportionality

Abstract. For the fatigue analysis of structures undergoing non-proportional stress histories, the critical plane approach has proven a physically meaningful and thus comprehensive method. However, procedures that accurately identify the critical plane are computationally very costly. In order to reduce computation times and to make full use of the critical plane approach an adaptive algorithm for the identification of the critical plane is presented in this work. The algorithm is based on the segmentation of a half sphere in segments of equal surface areas. Starting with a coarse mesh the algorithm refines only those segments that probably include the actual critical plane. This simple, yet very effective approach refers only to the accumulated damages of the segments and is hence suitable for every critical plane failure criterion. Depending on the discretisation level and used failure criterion reductions of up to 82 % in computational time can be expected without loss of accuracy, which is demonstrated by a fatigue analysis of a wind turbine's trailing edge adhesive joint.

1 INTRODUCTION

To analyse the fatigue damage of multiaxial, non-proportional stress histories the critical plane approach offers the opportunity to design components in a physically meaningful way. In contrast to proportional stress histories the failure criteria have to be evaluated on each material plane due to varying principal stress directions. Therefore the computational effort is very high, which often leads to a damage evaluation on a limited number of deterministically chosen material planes. The most damaged plane within the analysis is declared as the critical plane and is used for fatigue verification, see e.g. [1–4].

An intuitive way to find the critical plane is to discretise the surface of a half sphere in order to calculate the normal vectors on the material planes of interest. In this way a finite number of theoretically existing planes of a material point can be found and analysed,

since two diametrically opposite points on the surface of a complete sphere represent the same plane.

Discretising the half sphere using equal angle increments in altitude and longitude can serve as a first approach. However, the distribution of segments becomes irregular in this case, because of smaller segment sizes near the poles. Since the discretisation needs to be sufficiently fine at the equator, the mesh density becomes excessively fine at the poles, leading to huge computational costs.

Weber et al. [5] proposed the use of equal segment areas instead of equal angle increments. This yields to homogeneous discretisation densities across the entire half-sphere and reduces the computational cost effectively, see Tab. 1. Nevertheless, there is still the problem to define *a priori* an appropriate mesh density. The discretisation has to be fine enough to ensure that the critical plane is actually found. A fine segmentation leads to precise damage results. On the contrary, it results in extensive computational efforts, because areas with high damages are discretised in the same fashion as those with low damages.

The goal of this paper is to reduce the number of evaluated planes, and with it the computational cost, as much as possible without loss of accuracy. Therefore, a damage-based adaptive algorithm is developed. In order to demonstrate the performance of the proposed model in terms of accuracy and computational efficiency, we carry out a fatigue analysis of the trailing edge adhesive joint of a wind turbine rotor blade.

Table 1: Overall segment quantity required to discretise a half sphere using equal angle increments for both altitude and longitude or the equal areas approach according to Weber et al. [5], both depending on the selected discretisation.

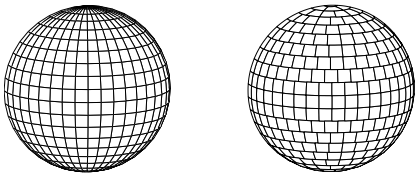

Discretisation (in deg.)	Total number of segments	
	equal increments	equal areas [5]
18.00	100	66
9.00	400	256
4.50	1600	1018
2.25	6400	4080

2 ADAPTIVE CRITICAL PLANE IDENTIFICATION

In this section the methodology of the adaptive critical plane identification is explained, followed by a detailed flowchart and setup options to reproduce the algorithm.

2.1 Methodology

The algorithm is based on a coarse Weber half sphere [5] whose segments are divided into four smaller rectangular segments within each refinement level in case they have the potential to contain the critical plane. This potential is expressed by means of a threshold $\mathscr{D}$ defined by

$$\mathscr{D} = \delta \cdot D_{max} \ , \tag{1}$$

where D_{max} is the maximum damage calculated in the previous refinement level and δ is a fraction that can be specified by the user. For the damage fraction it holds $0 \leq \ \delta \ \leq 1$. Following the analysis of every segment of the initial configuration ($\mathscr{L}_0$) only segments with damages exceeding the threshold $\mathscr{D}$ are refined. In that process the damage evaluation is always done for the centre of the rectangular segments. Table 2 visualises the adaptive refinement process using the Findley criterion [2, 6].

Table 2: Exemplary depiction of the adaptive refinement process. Figures and data are based on the analysis of the trailing edge adhesive joint of the IWT-7.5-164 [7] reference wind turbine rotor blade using the Findley criterion [2, 6]. The cumulative number of analysed segments is labelled $\sum$ Seg.

		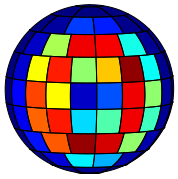	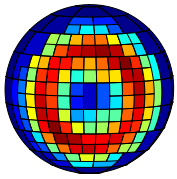	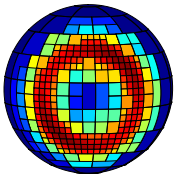	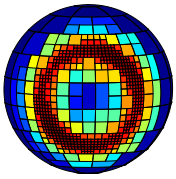
		$\mathscr{L}_0$	$\mathscr{L}_1$	$\mathscr{L}_2$	$\mathscr{L}_3$
Discr.	[°]	18.00	9.00	4.50	2.25
δ	[−]	0.750	0.750	0.875	0.975
$\sum$ Seg.	[−]	66	170	354	746

To limit computational costs in case of converging segment damages the algorithm is also equipped with a user defined damage tolerance ϵ. Only if the damage of a segment exceeds that of its parent segment[1], which is increased by the damage tolerance ϵ, it is passed to the next refinement level.

Depending on the initial discretisation, the actual critical plane might be located close to the edges of a previously eliminated segment. This is why segments adjacent to selected segments of refinement level $\mathscr{L}_0$ get partially refined assuring that the global optimum can be found. The partial refinement is done in a way that only those quarters of an adjacent segment are refined that share an edge with a previously selected segment.

2.2 Flowchart and setup options

The algorithm starts with the initial segmentation ($S_{initial}$) of the half sphere, which is specified by the user. Subsequently the damages ($D_{initial}$) and the user specified damage

[1] A parent segment is a segment that is refined in a refinement step. Hence, four refined segments share one parent segment.

threshold ($\mathscr{D}$) are calculated for the first iteration (refinement level $\mathscr{L}$), see Fig. 1.

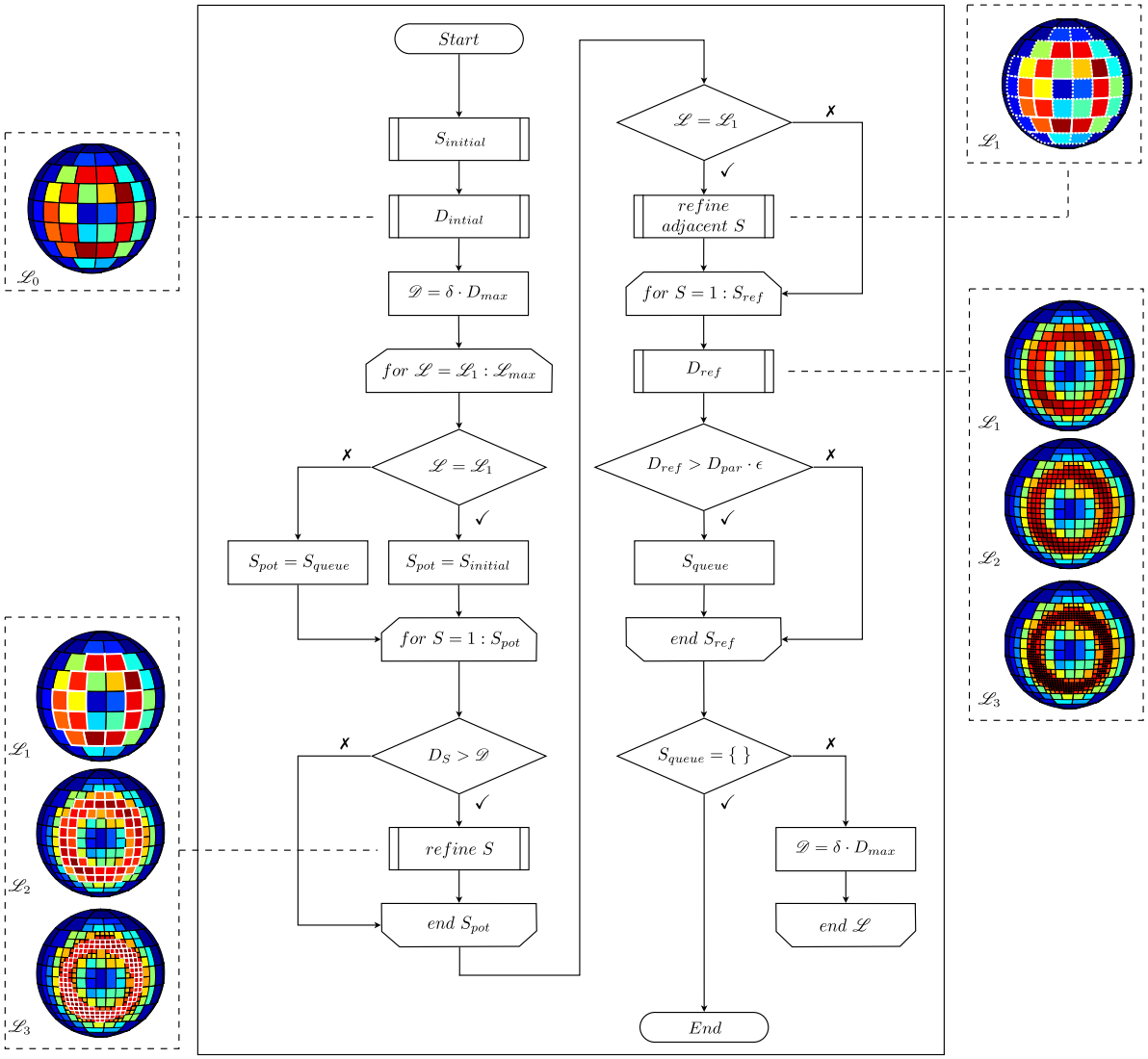

Figure 1: Flowchart of the proposed adaptive critical plane identification algorithm. Exemplary illustrations based on the analysis of a trailing edge adhesive joint of the IWT-7.5-164 [7] reference wind turbine rotor blade using the Findley criterion [2, 6]. Segments determined to be refined are highlighted with white edges. Dotted white edges are used in case of adjacent segments, which are partially refined.

Hereafter the refinement level loop is started. Within the first refinement level ($\mathscr{L}_1$) the number of segments that potentially comprise the critical plane (S_{pot}) equals the number of initial segments. Therefore an additional loop over S_{pot} is started looking for segment damages (D_S) bigger than the current threshold. If such a damage is found the corresponding segment is refined into four smaller segments. As an example segments found this way within the analysis of the trailing edge adhesive joint of a wind turbine

rotor blade (section 3) are highlighted with white edges in the lower left corner of Fig. 1 for three refinement levels. In $\mathscr{L}_1$ the segments adjacent to the previously refined ones are partially refined. In the upper right side of Fig. 1 these segments are highlighted with dotted white edges. To limit the computational effort only those quarters in direct contact to previously refined segments are refined. Now knowing the amount of refined segments (S_{ref}) a third loop is started in which the corresponding damages are calculated. Subsequently the damage of a refined segment is compared to the damage of its parent segment taking into account a user specified tolerance ϵ. This way only areas with non-converging damages are passed to the next refinement level by putting them into a queue (S_{queue}). In case the queue is empty, the algorithm stops the analysis. However, if the queue is not empty, a new damage threshold is calculated and the next refinement level is analysed. Since the algorithm itself refines segments purely based on damage values, it is applicable for any critical plane criterion. Moreover, it can be easily modified to fit the accuracy or execution time demands. Setup options for the algorithm including general recommendations are given in Tab. 3.

Table 3: Setup options of the adaptive critical plane identification algorithm with general recommendations. The damage fraction δ should be interpreted as a vector with individual values for each $\mathscr{L}$.

Variable	Recommendation
$S_{initial}$	equatorial width of $\pi/10$
$\mathscr{L}_{max}$	3 to 4 depending on $S_{initial}$
δ	[0.750, 0.875, 0.975] for $\mathscr{L}_{max} = 3$
ϵ	1.01

3 NON-PROPORTIONAL FATIGUE ANALYSIS

This section presents the non-proportional fatigue analysis of the trailing edge adhesive joint of the IWT-7.5-164 [7] reference wind turbine rotor blade using the proposed adaptive algorithm.

3.1 Finite element rotor blade model

The fatigue analysis in this work considers the trailing edge adhesive joint of the IWT-7.5-164 [7] reference wind turbine rotor blade. The finite element (FE) model of the blade was generated using the parameterised Model Creator and Analyzer (MoCA) developed at the Institute for Wind Energy Systems at Leibniz Universität Hannover. Within the meshing process shell elements are utilised to model the structural members made of fibre composite or sandwich materials. Solid elements are used in the trailing edge adhesive joint. In this work the analysis was limited to the radial sections of 34 m $\leq r \leq$ 74 m, where r is the local radius of a cross-section, see Fig. 2.

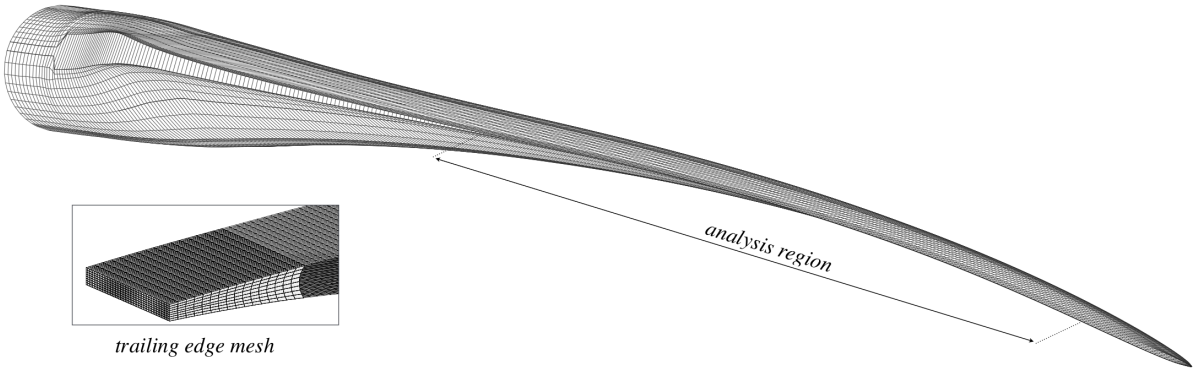

Figure 2: IWT-7.5-164 [7] reference wind turbine rotor blade FE mesh generated with MoCA. The trailing edge adhesive joint was implemented within the marked analysis region ranging from 34 m $\leq r \leq$ 74 m. A detailed view of the trailing edge mesh is presented on the left.

3.2 Methods within the fatigue analysis

To obtain accurate stress histories $\boldsymbol{\sigma}(t)$ for each element a reference stress state $\boldsymbol{\sigma}_{ref}$ is generated at first. This is done within a FE analysis using unit loads. The reference stress state is then combined with load histories $\mathbf{F}(t)$ in a linear superposition of scaled unit stress states, see [8]. The load histories are based on IEC guidelines [9] and were calculated using the coupled aero-servo-elastic code HAWC2 [10]. To generate statistically meaningful data each element stress history contains six individual sets including wind speed bins reaching from 3 to 25 m/s and three wind directions (-8°, 0°, 8°). Each bin includes $3 \cdot 10^4$ entries, so that a complete element stress history covers 414 sub-histories (6 sets, 3 directions, 23 wind speeds) and $1.242 \cdot 10^7$ entries in total.

For the fatigue assessment of non-proportional stress histories the critical plane approach is utilised. In general the analysis starts with the projection of $\boldsymbol{\sigma}(t)$ onto a potential critical plane with normal vector $\mathbf{n}$ resulting in a 3D traction vector $\mathbf{T_n}(t)$, which is composed of a 1D normal stress history perpendicular to the plane and an in-plane 2D shear stress history. To increase the computational efficiency the multiaxial Racetrack Filter (MRF) [2,11] can be applied to filter small amplitudes in $\mathbf{T_n}(t)$ leading to a reduced amount of data without a significant impact on the resulting damages.

The reduced stress history vector is then subjected to a rainflow counting scheme using the Modified Wang-Brown (MWB) algorithm [2, 12], which is able to account for multidimensional stress histories. Equivalent stresses of the resulting cycles such as the shear stress amplitudes of the 2D in-plane stress cycles are subsequently calculated based on the Polar Moment of Inertia method (PMOI) [2, 13–15]. Thereafter the damage of the currently analysed plane is calculated for every cycle in consideration of a critical plane damage criterion. In this paper, we employ the Findley damage criterion [2, 6]. The damage accumulation is assumed to be linear according to Palmgren and Miner [4]. The frequency of the wind speed is typically following a Weibull distribution. Hence, the annual fatigue damages in the adhesive joint are calculated using a Weibull distribution-based extrapolation of the computed damages for the individual wind speed bins. Fig. 3

summarises the methods used in the fatigue analysis in this work.

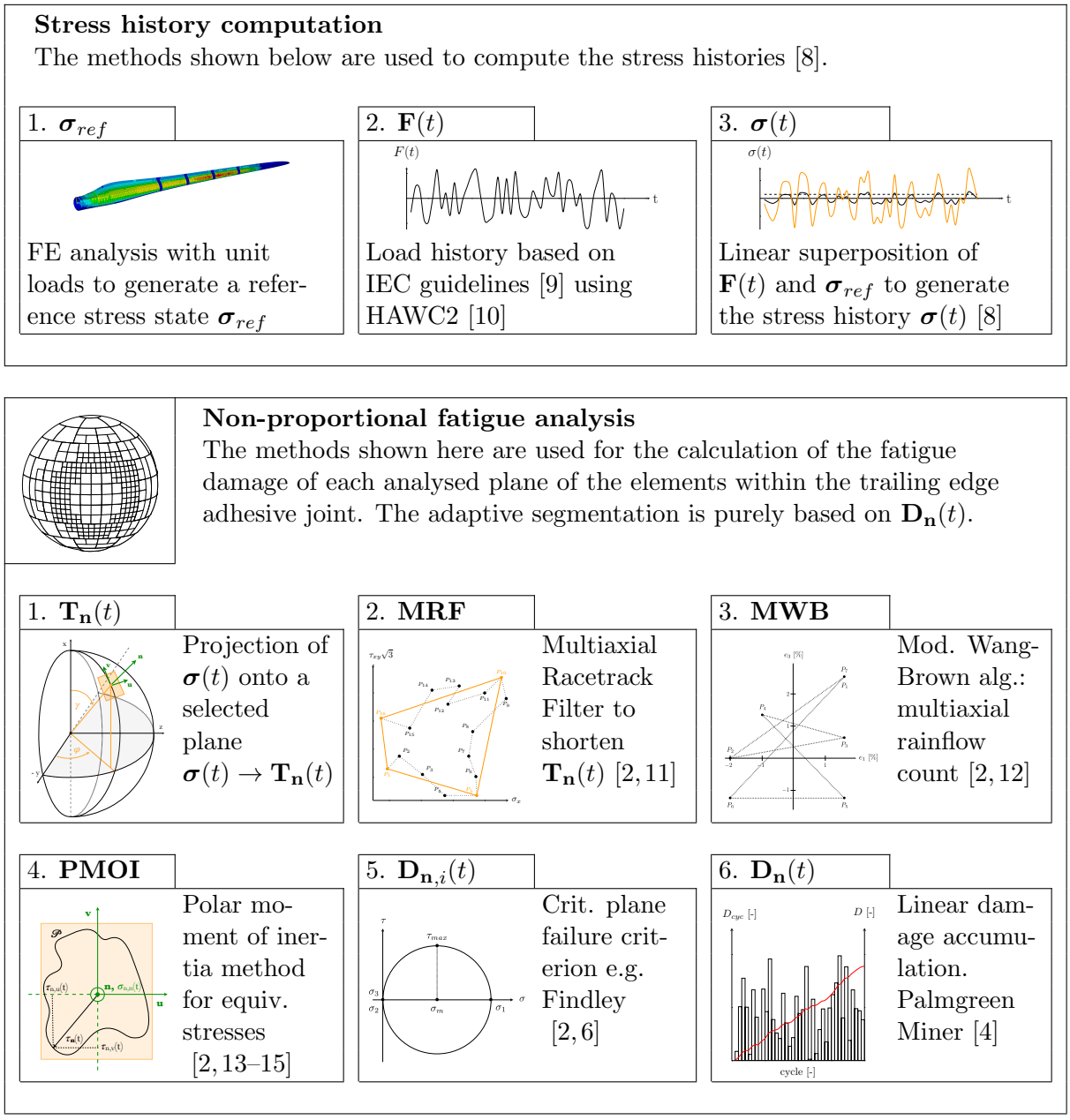

Figure 3: Methods used in the non-proportional fatigue analysis of the trailing edge adhesive joint of the IWT-7.5-164 [7] reference wind turbine rotor blade (illustrations are exemplary).

3.3 Results

To show the capability of the proposed algorithm, 75 element stress histories and 31,050 sub-histories, respectively, were analysed. Therein, the elements were equally spaced along the radial analysis region, see Fig. 2. Within the analysis we assumed that a static

1°-Weber [5] discretisiation (20,630 segments) can serve as a reference configuration and that a static 5°-Weber [5] discretisation (824 segments) can be considered for a state of the art critical plane analysis.

Figure 4 depicts the relative difference of the analysed segment quantity compared to the state of the art discretisation. On average (P_{50}) the algorithm reduces the amount of analysed planes by 72 %. Reductions for P_{85} are still at 35 % while the reduction of segments reaches $\Delta\text{Seg} = 82$ % for P_{25}.

In very rare occasions (0.06 %) the algorithm requires slightly more segments then the 5°-Weber [5] discretisation. This is the reason why the coordinate origin of Fig. 4 is slightly shifted to the right. However, we would like to emphasize that the damage results are more accurate in this particular and most other cases. Hence, the user will not have a disadvantage.

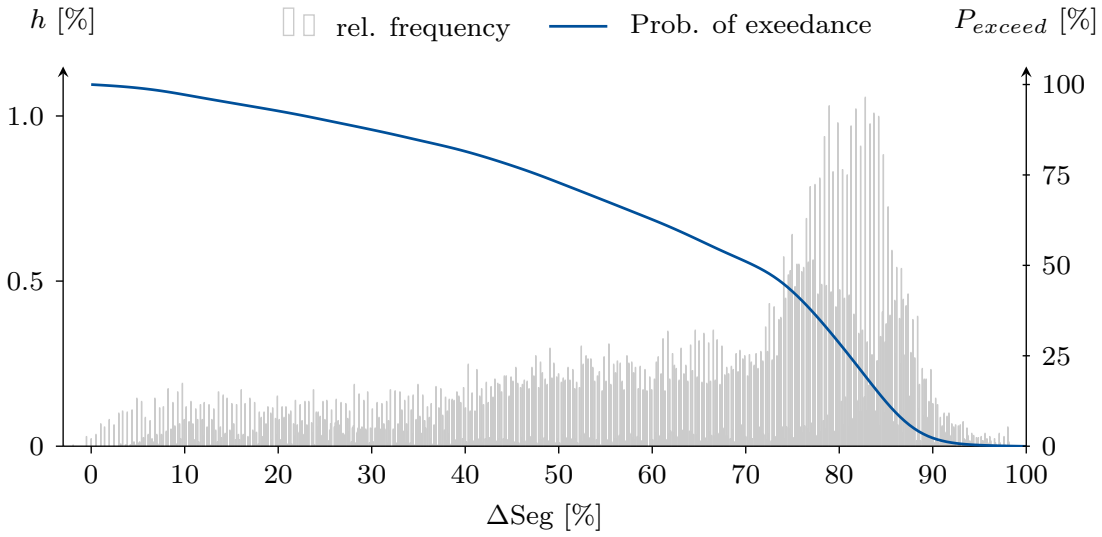

Figure 4: Efficiency of the critical plane identification using the proposed adaptive algorithm: The relative frequency (h in %, left scale) and the probability of exceedance (P_{exceed} in %, right scale) are plotted against the relative difference of the algorithm's segment quantity compared to the state of the art static 5°-Weber [5] discretisation which is denoted by ΔSeg.

Figure 5 shows the relative damage differences of both the adaptive algorithm and the state of the art configuration compared to the reference. It can be observed that the adaptive algorithm shows better accuracy than the state of the art discretisation. On average (P_{50}) the algorithm shows a damage deviation of -0.20 %, the static 5°-Weber [5] discretisation gives 0.87 % less accurate results than the reference. On account of the static reference discretisation there is also a 17.6 % chance to identify a higher damage than the one of the reference configuration using the adaptive algorithm. In case of the 5°-configuration this chance is about 2.9 % due to slightly different segment centre positions and critical plane coordinates, respectively.

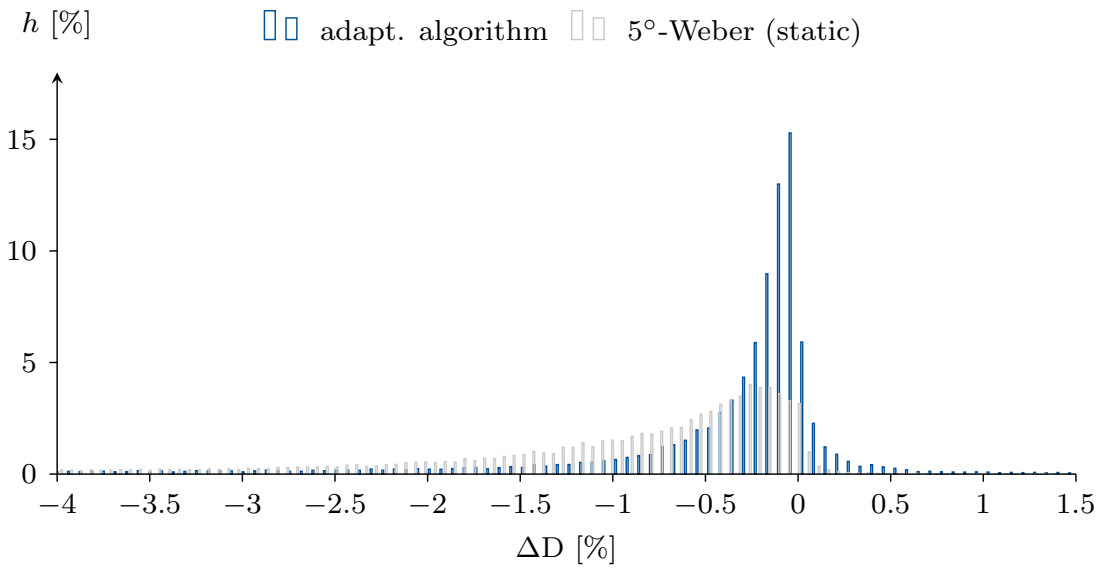

Figure 5: Accuracy of the adaptive algorithm and a static 5°-Weber [5] discretisation in comparison to a 1°-Weber discretisation, which was set as the reference solution.

4 CONCLUSIONS

In this manuscript, we presented an adaptive algorithm for the identification of the critical plane in a fatigue damage calculation. The algorithm can be combined with any critical plane-based fatigue criterion and is thus very user-friendly. A set of recommended parameters that control the performance of the algorithm has been given in the paper, which gives a good compromise between accuracy and computational costs. The analysis of the trailing edge adhesive joint of the IWT-7.5-164 reference rotor blade revealed that the algorithm saves 72 % in computational time on average (P_{50}) compared to a state of the art discretisation. Moreover, it has been shown that the adaptive algorithm is more accurate in calculating the fatigue damage at the same time. It can be concluded that the proposed algorithm reduces computational costs in critical plane-based fatigue analyses without major restrictions in accuracy, which was the goal of the developments.

ACKNOWLEDGEMENTS

The authors would like to acknowledge the financial support of the ECCOMAS scholarship.

REFERENCES

[1] D. F. Socie and G. B. Talyor, *Multiaxial Fatigue*, 1st Edition, Society of Automotive Engineers Inc., 2000.

[2] J. T. Pinho de Castro and M. A. Meggiolaro , *Fatigue Design Techniques Under Real Service Loads. Volume II - Low Cycle and Multiaxial Fatigue*, 1st Edition, CreateSpace Indepentent Publishing Platform, 2016.

[3] S. Suresh, *Fatigue of Materials*, 2nd Edition, Cambridge University Press, 2004.

[4] E. Haibach, *Betriebsfestigkeit - Verfahren und Daten zur Bauteilberechnung*, 3rd Edition, Springer-Verlag, 2006.

[5] B. Weber, B. Kenmeugne, J. Clement and J. Robert, Improvements of multiaxial fatigue criteria computation for a strong reduction of calculation duration. *Computational Material Science*, Vol. **15**, pp. 381–399, 1999.

[6] W. N. Findley, A Theory for the Effect of Mean Stress on Fatigue of Metals Under Combined Torsion and Axial Load or Bending. *Journal of Engineering for Industry*, pp. 301-306, 1959.

[7] A. Sevinc, M. Rosemeier, M. Bätge, R. Braun, F. Meng, M. Shan, D. Horte, C. Balzani, A. Reuter, O. Bleich, E. Daniele, P. Thomas and W. Popko, IWES Wind Turbine IWT-7.5-164 Rev. 2.5. Fraunhofer IWES, 2017.

[8] P. Noever-Castelos and C. Balzani, The impact of geometric non-linearities on the fatigue analysis of trailing edge bond lines in wind turbine rotor blades, *Journal of Physics: Conference Series*, Vol. **749**, 2016.

[9] IEC 61400-1, *International Standard: Wind Turbines - Part 1: Design requirements*, 3rd Edition, IEC Central Office, 2007.

[10] T. J. Larsen and A. M. Hansen, *How 2 HAWC2, the user's manual*, Risø-R-1597, Risø National Laboratory, 2015.

[11] H. Wu, M. A. Meggiolaro and J. T. Pinho de Castro, Validation of the multiaxial racetrack amplitude filter. *International Journal of Fatigue*, Vol. **87**, pp. 167-179, 2016.

[12] M. A. Meggiolaro and J. T. Pinho de Castro, An improved multiaxial rainflow algorithm for non-proportional stress or strain histories - Part II: The Modified Wang-Brown method. *International Journal of Fatigue*, Vol. **42**, pp. 194-206, 2012.

[13] M. A. Meggiolaro and J. T. Pinho de Castro, An improved multiaxial rainflow algorithm for non-proportional stress or strain histories - Part I: Enclosing surface methods. *International Journal of Fatigue*, Vol. **42**, pp. 217-226, 2012.

[14] M. A. Meggiolaro, J. T. Pinho de Castro and H. Wu, Generalization of the moment of inertia method to estimate equivalent amplitudes for simplifying the analysis of arbitrary non-proportional multiaxial stress or strain histories. *Acta Mechanica*, Vol. **227**, pp. 3261-3273, 2016.

[15] H. Wu, M. A. Meggiolaro and J. T. Pinho de Castro, Application of the Moment Of Inertia method to the Critical-Plane Approach. *Frattura ed Integrità Strutturale*, Vol. **38**, pp. 99-105, 2016.